**RESEARCH ARTICLE**

# Elaboration and characterization of Fe/C-doped lead dioxide-modified anodes for electrocatalytic degradation of Reactive Yellow 14

Sanaa El Aggadi[1] · Younes Kerroum[1] · Abderrahim El Hourch[1]

## Abstract

$Fe^{3+}$ and/or carbon black-doped $Ti/PbO_2$ electrodes were successfully synthesized via electrodeposition technology. The morphology and crystal structure of the electrodes were characterized by Scanning Electron Microscopy coupled with Energy Dispersive X-ray Spectroscopy (SEM/EDS) and X-ray Diffraction (XRD), respectively. Furthermore, Linear Sweep Voltammetry, Cyclic Voltammetry (CV), and Electrochemical Impedance Spectroscopy tests were also performed to analyze the electrochemical performance of the electrodes. The electrocatalytic activity of electrodes was examined by electrocatalytic oxidation of Reactive Yellow 14 (RY14) azo dye's model pollutant. The SEM showed that the morphology and size of $PbO_2$ particles are strongly affected by doping with $Fe^{3+}$ and carbon black. The EDS confirmed the existence of Fe and C elements. The XRD patterns show that samples were composed of higher content of $\beta$-$PbO_2$. $Ti/PbO_2$-0.1Fe (0.1 M $Fe^{3+}$ + 0 g C) electrode exhibits the highest oxygen evolution potential (1.64 V/SCE). The CV test indicated that the presence of the anodic peak at 1.45 V/SCE means that the oxidation of RY14 dye was easily achieved on the surface of all prepared electrodes. The Nyquist plots show the presence of two semicircles, one in the high-frequency domain describes the electron transfer process, while the second in the low-frequency domain explains the adsorption of the intermediate. $Ti/PbO_2$ and $Ti/PbO_2$-0.1Fe electrodes showed the best performance on degradation of RY14.

**Graphical Abstract**



---
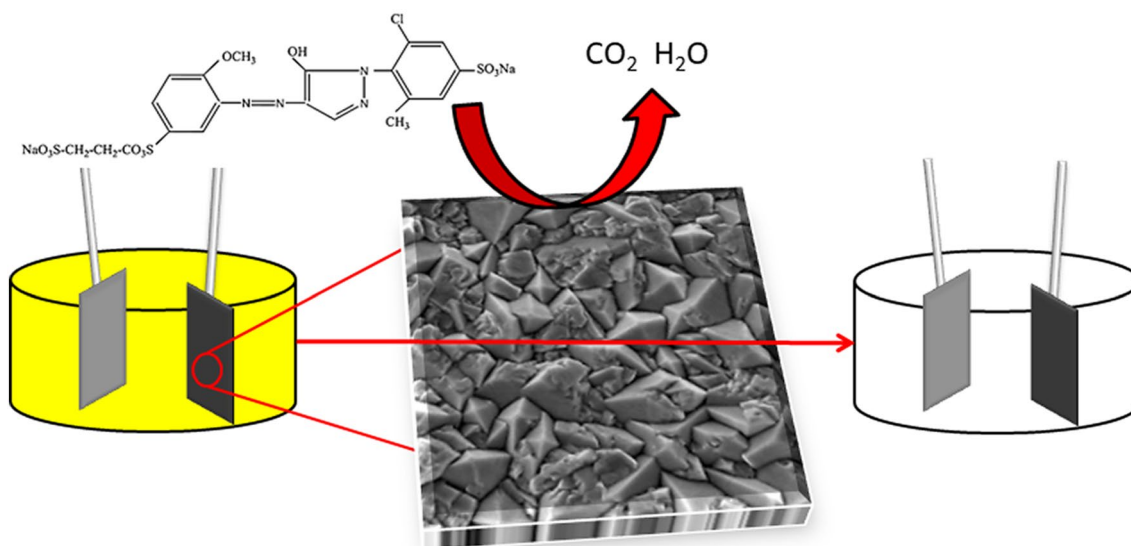
✉ Sanaa El Aggadi
  sanaa_elaggadi@um5.ac.ma

1   Department of Chemistry, Faculty of Sciences, Mohammed
    V University in Rabat, 4 Avenue Ibn Battouta, BP: 1014,
    Rabat, Morocco

# 1 Introduction

Worldwide, approximately 70% of the world's dye production corresponds to azo compounds, coming mainly from industries such as textiles or tanning, which are released every day [1, 2]. This kind of dyes has a complex chemical structure containing one or more azo groups (−N=N−) as a chromophore, connected to aromatic systems with lateral groups, including −OH, −SO$_3^-$, and −CH$_3$, among others [3]. In many cases, the wastewater generated by this industry is discharged into municipal wastewater treatment plants without any pretreatment [4]. The negative effects of azo dyes on both humans and aquatic life have led to urgent calls for the treatment of effluents containing azo dyes in order to remove them or to turn them into safe and useful products [5, 6]. To treat these wastewaters effectively, the so-called advanced oxidation processes (AOPs) are widely applied. The AOP techniques include photocatalysis, Fenton oxidation, electrocatalytic oxidation, and a combination of these processes [7, 8].

Electrocatalytic oxidation technology represents an interesting approach for the treatment of hazardous, toxic, and highly concentrated organic wastewater due to its high efficiency, ease of control, versatility, low time consumption, and environmental sustainability [9–11]. During the electrocatalytic process, the anode material is a key factor in the oxidation efficiency of organic pollutants [12, 13]. Several types of electrodes have been studied, including platinum [14], graphite [15, 16], MnO$_2$ [17], PbO$_2$ [18, 19], RuO$_2$ [20], IrO$_2$ [21], SnO$_2$ [22, 23], and boron-doped diamond [24]. Among these electrodes, PbO$_2$ is one of the best candidates widely used in electrocatalysis due to its high oxygen evolution potential (OEP), good corrosion resistance, low price, and high electrocatalytic activity [10]. However, due to its fragility and ease of deactivation [25], many attempts have been made to improve the performance of the PbO$_2$ electrode. A frequently used method consists in doping the PbO$_2$ layer with some materials, such as cations (Bi$^{3+}$ [26], Fe$^{3+}$ [27], Cu$^{2+}$ [28], Zr$^{4+}$ [29], Ce$^{3+}$ [30], and Co$^{2+}$ [31]), anions (F$^-$ [32] and [Fe(CN)$_6$]$^{3-}$ [33]), surfactants (cetyltrimethylammonium bromide [34], sodium dodecyl sulfate [35, 36], sodium dodecyl benzene sulfonate [37], polyvinylidene fluoride [38], polyethylene glycol [39]), ionic liquids [40], carbon nanotubes [41], etc. The results show that the modified PbO$_2$ electrode exhibits excellent electrocatalytic activity and stable performance.

Our investigation focuses on the modification of the PbO$_2$ electrode. In this paper, we suggest a new method of modification of PbO$_2$ electrode in order to increase the electrochemical activity and the lifetime of PbO$_2$ electrode. It is widely known that carbon has a unique structure, extraordinary chemical, mechanical, and electronic properties and has been widely studied in fuel cells, supercapacitors, and biosensors [41, 42]. It is widely known that carbon has extraordinary chemical, a unique structure, extraordinary chemical, electronic, and mechanical properties [43, 44], and has been widely studied in fuel cells, biosensors, and supercapacitors. At the same time, some investigations have demonstrated that Fe doping in PbO$_2$ electrodes can achieve better coating quality and higher electrocatalytic performance [45]. But until now, there are no reports on the modification of PbO$_2$ electrode by co-doping carbon and iron.

In this work, lead dioxide electrodes undoped and doped with Fe$^{3+}$ and/or carbon black were prepared by electrodeposition. The morphology, crystalline structure, and electrochemical performances were characterized. Reactive Yellow 14 (RY14) azo dye (C$_{20}$H$_{19}$ClN$_4$Na$_2$O$_{11}$S$_3$, CAS number: 18976-74-4) was chosen as the model pollutant for electrocatalytic oxidation to evaluate electrochemical activity of the electrodes.

# 2 Experimental

## 2.1 Materials

Pb(NO$_3$)$_2$, Fe(NO$_3$)$_3$·9H$_2$O, NaOH, and C$_2$H$_2$O$_4$ were purchased from VWR Prolabo Chemicals. Na$_2$SO$_4$ was supplied by Panreac. KNO$_3$ was obtained from Janssen Chimica, Pure (> 99.9%). Carbon black was purchased from Alfa Aesar. Titanium plates with 0.1 mm thickness were purchased from Eszkozok Tools (Zhejiang, China) and used as the substrate. Doubly deionized water was used for the preparation of all solutions and Ti plate washing. All of the experiments were performed at 20 °C.

## 2.2 Electrode preparation

A titanium plate was used as substrate. It was initially pretreated by polishing with different types of sandpaper (Grit No. 100, 400, 600, 1200) and cleaned with double-distilled water to remove sand particles. Afterward, the plate was immersed in a 40% sodium hydroxide solution (50 °C) for 2 h to remove organic residues from the surface, and then it was placed in a slightly boiling 10% oxalic acid, etched for 2 h and washed with distilled water. Finally, in order to avoid the formation of TiO$_2$, the titanium plate was stored in a 1% oxalic acid solution. This treatment should, therefore, strengthen the bond strength between the electrode surface and the oxide coating, improve the conductivity of the titanium plate, and extend the lifetime of the electrode [42, 43]. PbO$_2$ was deposited galvanostatically on

**Table 1** Name and composition of the prepared electrodes

| Electrode | Composition |
|---|---|
| Ti/PbO$_2$ | 0 M Fe$^{3+}$ + 0 g C |
| Ti/PbO$_2$-0.05Fe | 0.05 M Fe$^{3+}$ + 0 g C |
| Ti/PbO$_2$-0.1Fe | 0.1 M Fe$^{3+}$ + 0 g C |
| Ti/PbO$_2$-0.2Fe | 0.2 M Fe$^{3+}$ + 0 g C |
| Ti/PbO$_2$-0.05C | 0 M Fe$^{3+}$ + 0.05 g C |
| Ti/PbO$_2$-0.1Fe-0.05C | 0.1 M Fe$^{3+}$ + 0.05 g C |

the pretreated titanium substrate. The deposition solution (30 mL) was composed of 0.2 M Pb(NO$_3$)$_2$ and 0.1 M KNO$_3$ solution. The deposition processes were carried out at room temperature between 5 and 10 min, and the current density was controlled at 20 mA cm$^{-2}$. The electrodes were coated in the absence and presence of different concentrations of Fe$^{3+}$ (0.05 M, 0.1 M, and 0.2 M) and/or carbon black 0.05 g. The fabricated electrodes were marked as Ti/PbO$_2$, Ti/PbO$_2$-0.05Fe, Ti/PbO$_2$-0.1Fe, Ti/PbO$_2$-0.2Fe, Ti/PbO$_2$-0.05C, and Ti/PbO$_2$-0.1Fe-0.05C for 0 M Fe$^{3+}$ + 0 g C, 0.05 M Fe$^{3+}$ + 0 g C, 0.1 M Fe$^{3+}$ + 0 g C, 0.2 M Fe$^{3+}$ + 0 g C, 0 M Fe$^{3+}$ + 0.05 g C, and 0.1 M Fe$^{3+}$ + 0.05 g C, respectively (Table 1), dependent on the electrode fabricated in different concentrations of Fe(NO$_3$)$_3$•9H$_2$O and 0.05 g carbon black.

## 2.3 Electrode characterization

The surface morphology of the Ti/PbO$_2$ electrodes was observed by a scanning electron microscopy (SEM, JEOL JSM-IT 100) at an accelerating voltage of 20 kV.

The composition and crystalline structure of the coatings were characterized by Energy Dispersive X-ray Spectroscopy (EDS) and X-ray diffraction (XRD, LABXXRD-6100 SHIMADZU) using Kα radiation ($\lambda = 1.5406$ Å) in the 2θ range of 10°–70°. The X-ray tube was operated at 40 kV with a Cu target.

For electrochemical characterization of the prepared films, three-electrode cell configuration is connected to the PGZ 301 electrochemical workstation driven by VoltaMastrer 4 software. Ti/PbO$_2$, Ti/PbO$_2$-0.05Fe, Ti/PbO$_2$-0.1Fe, Ti/PbO$_2$-0.2Fe, Ti/PbO$_2$-0.05C, and Ti/PbO$_2$-0.1Fe-0.05C were used as working electrode with an active surface of 1 cm$^2$, a Ti plate was served as the auxiliary electrode and saturated calomel electrode (SCE) as the reference electrode. The measure of linear sweep voltammetry (LSV) was performed in 0.1 M Na$_2$SO$_4$ solution at the scan rate of 10 mV s$^{-1}$ from 0 to 3 V. Cyclic voltammetry (CV) was used to study the electrochemical behavior of the prepared electrodes using a 10$^{-2}$ M RY14 in 0.1 M Na$_2$SO$_4$ solution as the supporting electrolyte and scan rate of 100 mV s$^{-1}$

and potential range from 0 to 1700 mV. Electrochemical impedance spectroscopy (EIS) measurements were carried out in a range of 100 kHz–0.1 Hz at a potential of 0 V/SCE with a sine wave of 5 mV amplitude.

## 2.4 Electrocatalytic oxidation performance of the electrodes

The electrocatalytic oxidation activity of the prepared electrodes was evaluated by electrolysis of RY14. The experiments were carried out by the PGZ 301 electrochemical workstation in a 250 mL undivided electrochemical reactor. Each prepared electrode was used to electrolyze a solution containing 0.1 mM of RY14 dye in 0.1 M Na$_2$SO$_4$. The solution was kept under agitation using a magnetic stirrer. The experiments were carried out at room temperature (20 °C) for 120 min. During the experiments, samples were taken from the electrolytic cell every 20 min for UV–VIS analysis (Analytik Jena, Specord 210 plus). The maximum adsorption wavelength of RY14 dye is 410 nm. The color removal efficiency of RY14 in electrochemical oxidation can be calculated as follows [44]:

$$\text{Color removal efficiency}(\%) = \frac{A_0 - A_t}{A_0} \times 100\%, \quad (1)$$

where $A_0$ and $A_t$ are the absorbance value at an initial time and time $t$, respectively.

## 3 Results and discussion

### 3.1 Surface morphology of Ti/PbO$_2$ electrodes

Figure 1 shows SEMs of PbO$_2$ prepared from solutions containing 0.2 M Pb(NO$_3$)$_2$ and 0.1 M KNO$_3$ at 20 mA cm$^{-2}$ on the surface of Ti electrode in the absence and presence of Fe$^{3+}$ and/or C. Figure 1a shows the morphology of prepared Ti/PbO$_2$ in the absence of Fe$^{3+}$ and C. As is obvious, the morphology of the surface layer of the Ti/PbO$_2$ electrode is rough with typical pyramidal shapes, as well as some damage and cracks have been observed on the surface, which was similar to the earlier reports [33, 38, 45]. Figure 1b–d presents the morphology of lead dioxide deposited on the surface of Ti electrode from the deposition solution containing different concentrations of Fe$^{3+}$ ions. As can be seen, at low Fe$^{3+}$ concentration (0.05 M), the electrode lost its pyramidal shape and a uniform structure with well-distributed globular particles arranged in rice shape is deposited on the electrode surface (Fig. 1b). After adding (0.1 M) Fe$^{3+}$ to the deposition solution, the modified Ti/PbO$_2$-0.1Fe has a higher adherence to the electrode surface than that of sample prepared in the absence of Fe$^{3+}$ ions and still had the pyramidal structure,

**Fig. 1** SEM images of **a** Ti/PbO$_2$, **b** Ti/PbO$_2$-0.05Fe, **c** Ti/PbO$_2$-0.1Fe, **d** Ti/PbO$_2$-0.2Fe, **e** Ti/PbO$_2$-0.05C, **f** Ti/PbO$_2$-0.1Fe-0.05C electrodes
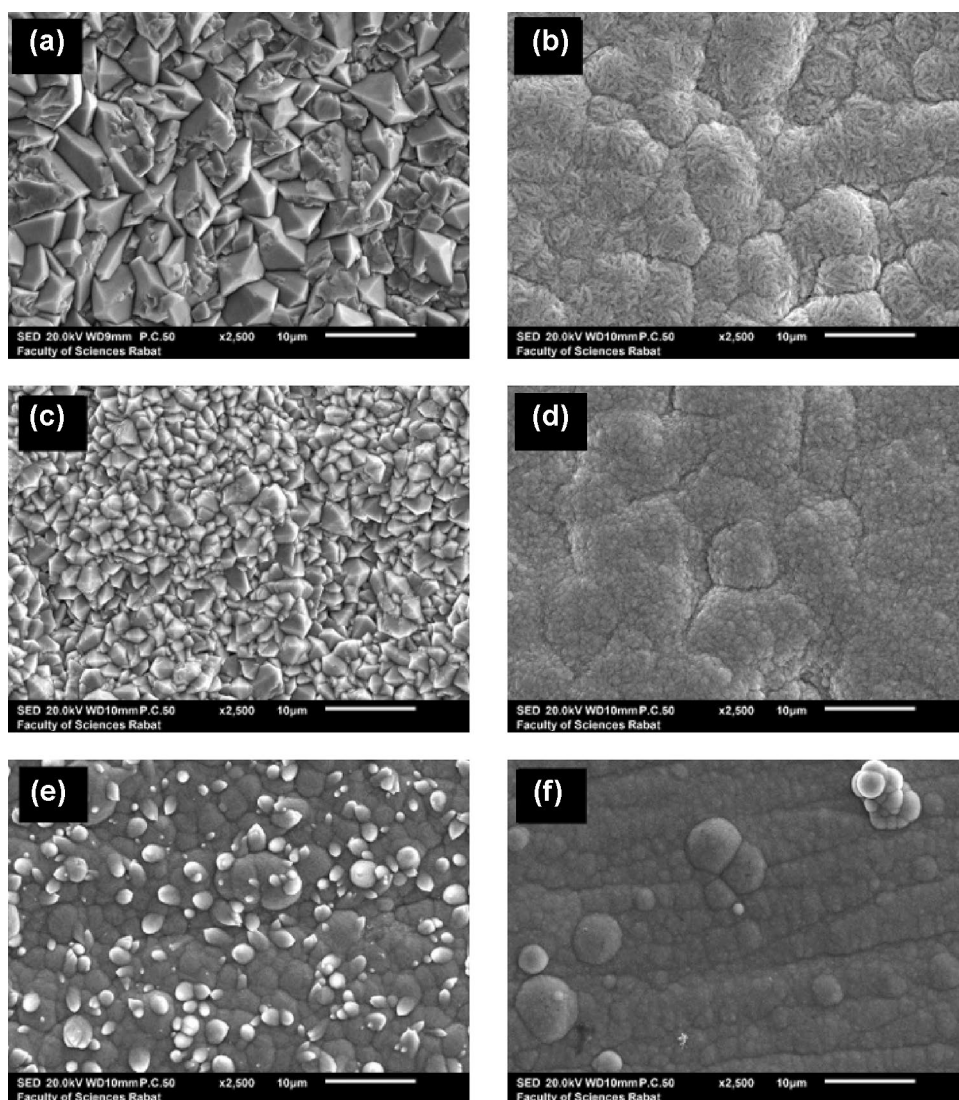


but with smaller size, ordered, uniform, and smoother than the unmodified electrode (Fig. 1c). Further increase in Fe$^{3+}$ concentration up to 0.2 M resulted in smaller, globular-shaped PbO$_2$ particle structures with obvious boundaries (Fig. 1d). Figure 1e shows the influence of adding 0.05 g of carbon black on the morphology of PbO$_2$ electrodeposited on the surface of the Ti electrode. A rice shape structure like that found in Fig. 1b but with smaller size is observed. Figure 1f shows the influence of the addition of a mixture of 0.1 M Fe$^{3+}$ and 0.05 g of carbon black on the morphology of the PbO$_2$ electrodeposited on the surface of the Ti electrode. A uniform structure is observed consisting of a pileup-pellet pattern with an undefined boundary and the smallest globular particles [28, 39, 46].

The EDS analysis results for the entire electrodes are shown in Fig. 2. From the EDS spectrums, it could be seen that the elements Pb, O, Fe, and C were detected by EDS. Moreover, with the increase of Fe$^{3+}$ doping amount, the content of Fe element was gradually increased from 0.41 to 1.89% (atom %). Also, the addition of 0.1 M Fe$^{3+}$ increases the amount of C doping from 12.87 to 33.28% (atom %). From the above results, it was proved that Fe and C elements were successfully and uniformly doped into the PbO$_2$ electrodes. Moreover, no other elements were detected, indicating that the surface of the electrodes was completely covered by the PbO$_2$ layer.

## 3.2 Structure of Ti/PbO$_2$ electrodes

Figure 3 shows XRD patterns of the different modified Ti/PbO$_2$ electrodes. The crystal structure of the Ti/PbO$_2$ electrode prepared in the absence of Fe$^{3+}$ consisted of a mixture of two common crystallographic structures, namely the forms α- (orthorhombic) and β-(tetragonal) with a higher content of β-PbO$_2$, which can be identified by its intense peaks, namely, (101 at 31.74°), (211 at 49.03°),
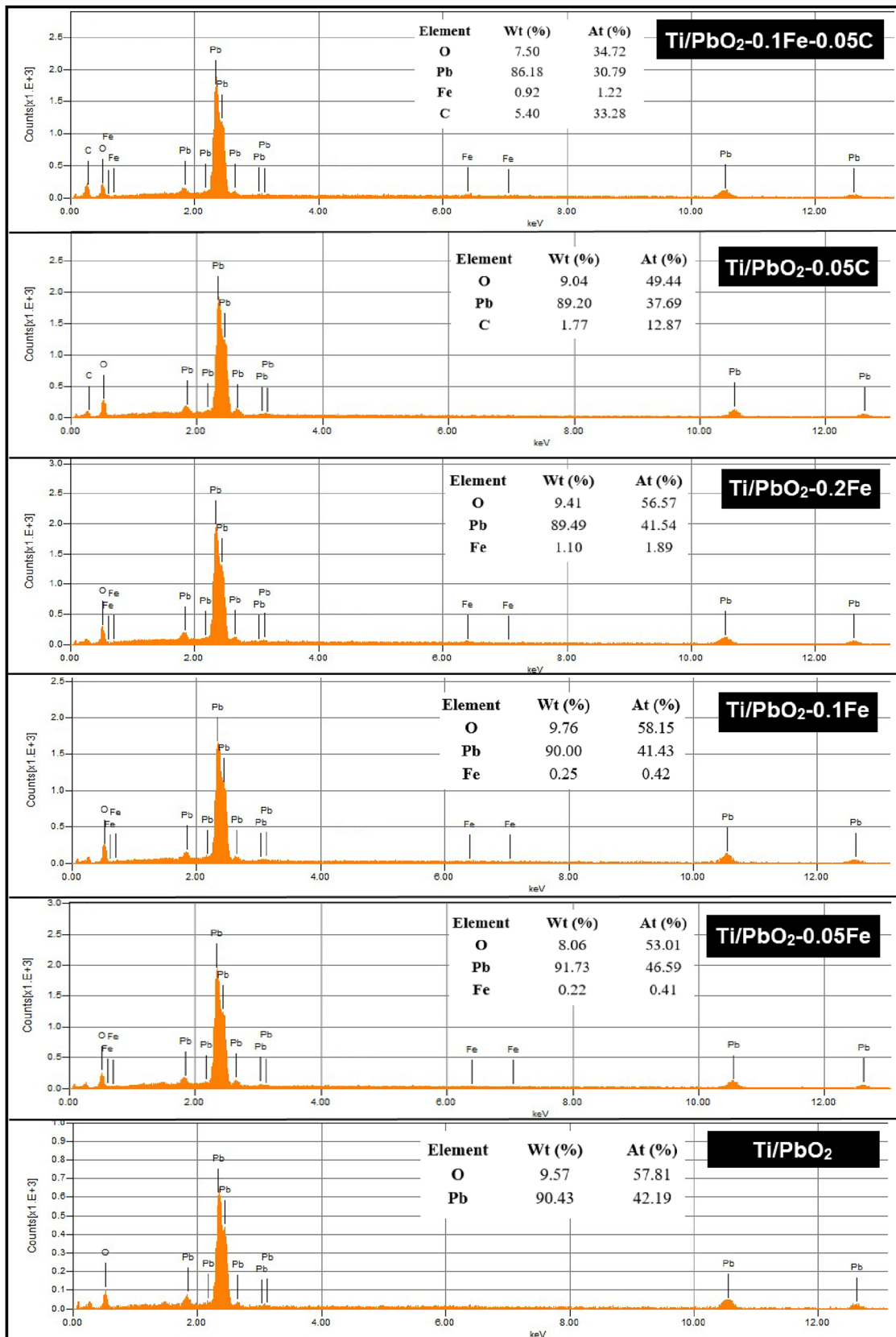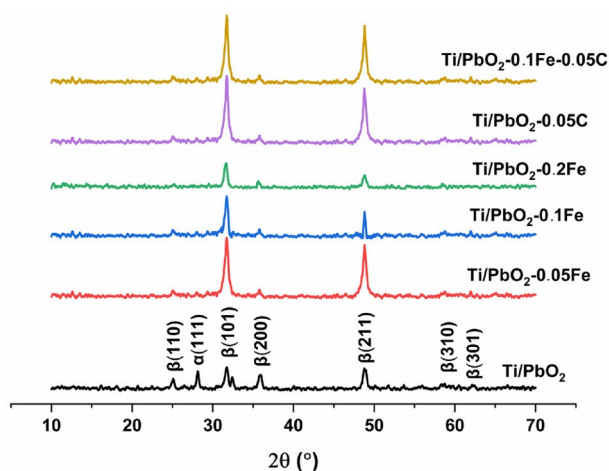
**Fig. 2** EDS analyses of the prepared electrodes

**Fig. 3** XRD patterns of the Ti/PbO₂ electrodes

**Table 2** Particle size calculated from XRD data

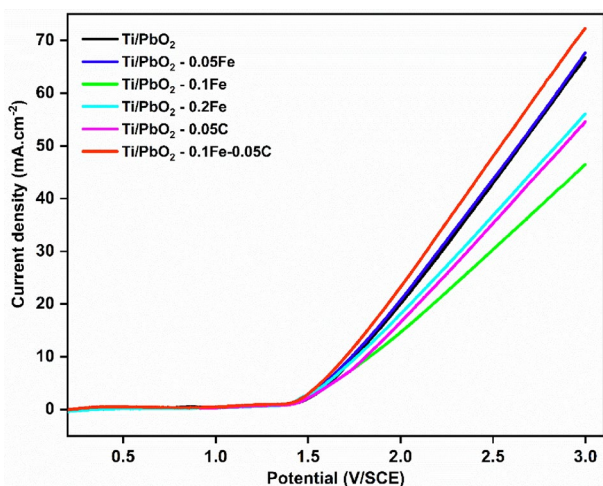| Sample | Particle size (nm) |
| --- | --- |
| Ti/PbO₂ | 22.83 |
| Ti/PbO₂-0.05Fe | 15.71 |
| Ti/PbO₂-0.1Fe | 18.01 |
| Ti/PbO₂-0.2Fe | 16.43 |
| Ti/PbO₂-0.05C | 14.79 |
| Ti/PbO₂-0.1Fe-0.05C | 14.72 |



**Fig. 4** LSV curves of different Ti/PbO₂ electrodes in 0.1 M Na₂SO₄ solution, scan rate: 10 mV s⁻¹

(200 at 36.2°), and (110 at 25.4°). However, only a single peak α-PbO₂ (111 at 28.32°) is observed. After the introduction of $Fe^{3+}$ in the electrochemical deposition solution, peaks such as β(110) and α(111) disappeared and no new peaks corresponding to Fe were detected. The predominant

phases were always β-PbO₂ (β(101) and β(211)). The addition of carbon black alone or with $Fe^{3+}$ (0.1 M) to the electrodeposition solution shows no new peak. It can be said that the doping of PbO₂ with Fe/C has not led to the appearance of a new phase. This means that iron and carbon could exist as an amorphous phase. This result was also obtained by Yang et al. who were able to confirm the presence of β-phase only in the XRD analysis of Bi-PbO₂ modified with different concentrations of polyethylene glycol (PEG) [39].

Table 2 provides information on the grain size evolution calculated from the X-ray line broadening of the (101) reflections using the Debye–Scherrer equation (Eq. 2) [47]:

$$D = \frac{K\lambda}{\beta \cos\theta},\tag{2}$$

where $D$ is the crystallite size, $\lambda$ is the X-ray wavelength, $\beta$ is the full width at half maximum of the peak, and $\theta$ is the diffraction angle.

It can be seen that doping PbO₂ with different concentrations of iron and carbon decreases the size of the electrodeposited particles.

## 3.3 Linear sweep voltammetry (LSV)

A high oxygen evolution potential (OEP) is highly recommended in the development of electrode material for wastewater treatment [48]. The OEP of the electrodes was determined using LSV. Figure 4 shows the LSV of different Ti/PbO₂ electrodes in 0.1 M Na₂SO₄ solution with a scan rate of 10 mV s⁻¹ between 0 and 3 V/SCE at room temperature (20 °C). Based on the polarization curves, the unmodified Ti/PbO₂ electrode had an OEP value of 1.61 V/SCE, which was close to other studies [49, 50]. The OEPs of the modified lead dioxide electrode are 1.60 V/SCE, 1.64 V/SCE, 1.60 V/SCE, 1.61 V/SCE, and 1.57 V/SCE, respectively, for Ti/PbO₂-0.05Fe, Ti/PbO₂-0.1Fe, Ti/PbO₂-0.2Fe, Ti/PbO₂-0.05C, and Ti/PbO₂-0.1Fe-0.05C, indicating that the addition of 0.1 M $Fe^{3+}$ has slightly increased the OEP of the electrode. Higher OEP contributed to reducing the occurrence of oxygen evolution and enhanced the formation of hydroxyl radicals [38, 46], resulting in increased oxidation efficiency and decreased energy consumption.

## 3.4 Cyclic voltammetry

Cyclic voltammetry was used to test the electrocatalytic activity of Ti/PbO₂ electrodes for RY14 oxidation. With the cyclic voltammetry technique, the oxidation of the pollutants is attributed to the direct transfer of electrons from the pollutants onto the electrodes. The cyclic voltammograms of 0.1 M Na₂SO₄ media with and without 10⁻² M RY14 on
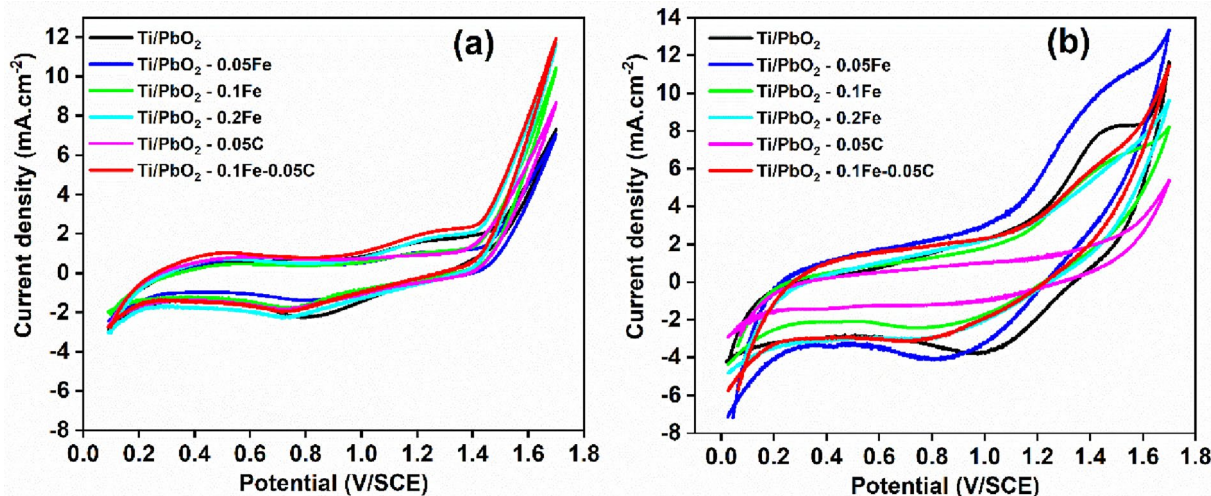
**Fig. 5** Cyclic voltammograms of different Ti/PbO$_2$ electrodes measured in **a** 0.1 M Na$_2$SO$_4$ and **b** 0.1 M Na$_2$SO$_4$ containing $10^{-2}$ M RY14 dye, scan rate: 100 mV s$^{-1}$
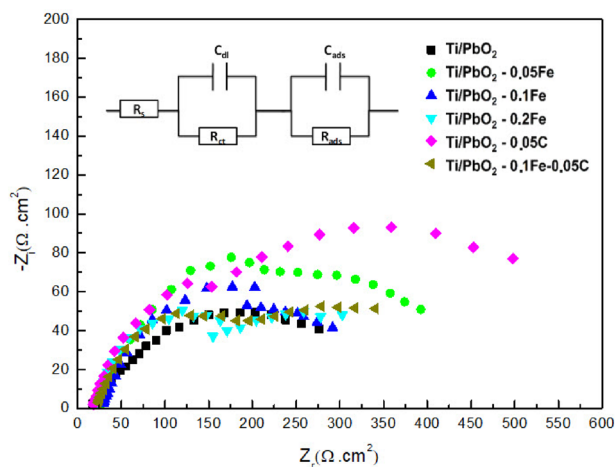


**Fig. 6** Nyquist plots of Ti/PbO$_2$ electrodes and equivalent circuit model (the inset) in 0.1 M Na$_2$SO$_4$ solution

the different prepared electrodes at a scan rate of 100 mV s$^{-1}$ within a potential range of 0 to 1.7 V/SCE are presented in Fig. 5. As we can see, in the blank electrolyte (Fig. 5a), there is no anodic peak except the one formed by the water discharge for all electrodes. After RY14 dye was added to the blank solution (Fig. 5b), a broad anodic peak at about 1.45 V/SCE appeared. In comparison to the cyclic voltammograms in the blank solution, it was clear that the anodic peak at 1.45 V/SCE depended on the oxidation of RY14 dye. The oxidation potential of RY14 was lower than the oxygen evolution potential, indicating that the oxidation process was due to direct electron transfer.

## 3.5 Electrochemical impedance spectroscopy (EIS)

Figure 6 shows the Nyquist plots of freshly prepared Ti/PbO$_2$ electrodes electrodes in 0.1 M Na$_2$SO$_4$ solution over a range of 100 kHz–0.1 Hz with a sine wave of 5 mV amplitude. The Nyquist plots show the presence of two semicircles, one in the high-frequency domain describes the electron transfer process, while the second in the low-frequency domain explains the adsorption of the intermediate. As shown in Fig. 6, the impedance of the Ti/PbO$_2$ anode is lower than that of the modified Ti/PbO$_2$ electrode, implying that the element-doped electrode disadvantages the electrochemical reaction process. The impedance parameters were extracted using the equivalent circuit (EC) inserted in Fig. 6. $R_s$ is the solution resistance, $C_{dl}$ represents the double-layer capacitance, $R_{ct}$ describes the charge transfer resistance, $C_{ads}$ and $R_{ads}$ are the capacitance and resistance generated by the adsorption of the intermediate on the electrode surface.

In addition, the parameters of EIS data are adjusted and rearranged in Table 3. In this study, the polarization resistance ($R_p$) was used to explore the effect of doped elements on the electrochemical reaction process of Ti/PbO$_2$ electrode. This parameter includes all the effects that occur during an electrochemical process. From Table 3, it can be observed that the anodes doped with 0.05 g carbon and 0.05 M Fe$^{3+}$ had high $R_p$, with the values of 637.90 Ω cm$^2$ and 456.90 Ω cm$^2$, respectively. In contrast, the other prepared anodes have an $R_p$ close to the PbO$_2$ electrode, especially for the one doped with 0.1 M Fe$^{3+}$. Moreover, we notice that the polarization resistance decreases significantly by adding 0.1 M Fe$^{3+}$ to the prepared carbon-doped anode, which demonstrates the positive effect of Iron in promoting the electrochemical reaction process in the presence of carbon.

**Table 3** Impedance parameters of Ti/PbO$_2$ electrodes

| | $R_{ct}$ ($\Omega$ cm$^2$) | $C_{dl}$ ($\mu$F cm$^{-2}$) | $R_{ads}$ ($\Omega$ cm$^2$) | $C_{ads}$ (mF cm$^{-2}$) | $R_{p}$ ($\Omega$ cm$^2$) |
|---|---|---|---|---|---|
| Ti/PbO$_2$ | 12.09 | 1.66 | 351.40 | 0.32 | 363.49 |
| Ti/PbO$_2$-0.1Fe | 20.02 | 5.02 | 352.40 | 0.05 | 372.42 |
| Ti/PbO$_2$-0.05Fe | 118.90 | 1.20 | 338.00 | 0.26 | 456.90 |
| Ti/PbO$_2$-0.2Fe | 166.60 | 19.10 | 233.10 | 1.71 | 399.70 |
| Ti/PbO$_2$-0.05C | 174.20 | 14.40 | 463.70 | 0.77 | 637.90 |
| Ti/PbO$_2$-0.1Fe-0.05C | 110.00 | 1.03 | 325.80 | 1.22 | 435.80 |
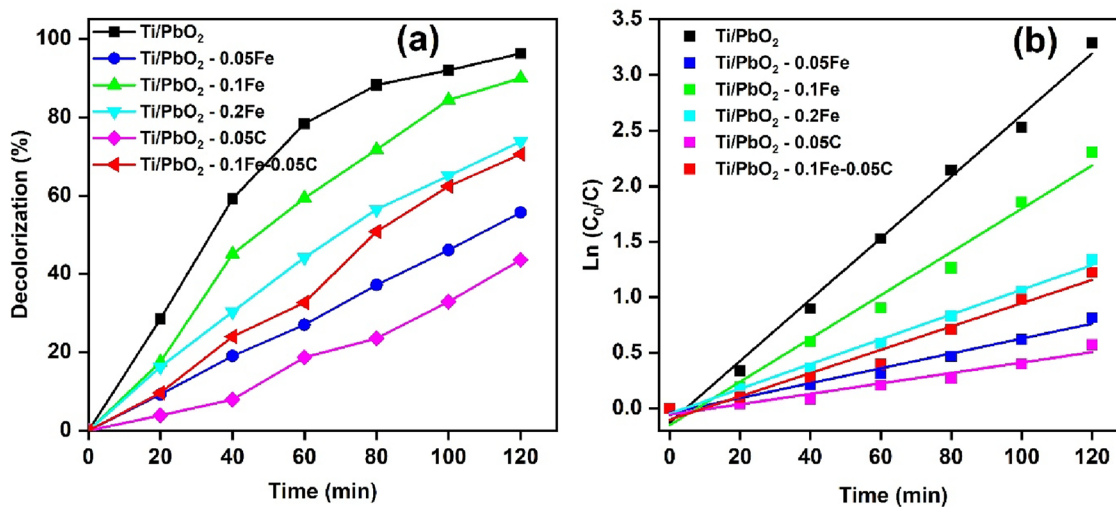


**Fig. 7** **a** Performance of Ti/PbO$_2$ electrodes for RY14 degradation, **b** pesudo-first-order kinetics for RY14 oxidation [Conditions: current density: 200 mA cm$^{-2}$; $V$ = 250 mL; (RY14) = 0.1 mM; electrolyte: 0.1 M Na$_2$SO$_4$]

## 3.6 Electrocatalytic oxidation of RY14 dye

The electrocatalytic activity of the Ti/PbO$_2$ electrodes was evaluated via electrocatalytic elimination of RY14 under galvanostatic condition at a current density of 200 mA cm$^{-2}$ for 120 min in 0.1 M Na$_2$SO$_4$ solution. Figure 7a shows the percentage of RY14 decolorization as a function of time. It can be seen that the decolorization rate reaches more than 90% using Ti/PbO$_2$ and Ti/PbO$_2$-0.1Fe electrodes after 120 min of electrolysis, while it was more than 70% using Ti/PbO$_2$-0.2Fe and Ti/PbO$_2$-0.1Fe-0.05C electrodes. According to these results, it can be said that the Ti/PbO$_2$ and Ti/PbO$_2$-0.1Fe electrodes showed the highest activity for color removal. However, the Ti/PbO$_2$ electrode does not hold well on the electrode, it deteriorates with time. The oxidation of the complex azo dye molecule results in intermediates with low molecular weight like aliphatic and aromatic compounds. They are formed by displacement of the chromophore functional group and subsequent oxidation of the organic compounds to carbon dioxide and organic acids (carboxylic

**Table 4** The kinetics for the electrochemical degradation of RY14 (electrolysis time: 2 h)

| Electrode | $K_{app}$ (min$^{-1}$) | $R^2$ |
|---|---|---|
| Ti/PbO$_2$ | 0.027 | 0.99 |
| Ti/PbO$_2$-0.05Fe | 0.006 | 0.98 |
| Ti/PbO$_2$-0.1Fe | 0.020 | 0.99 |
| Ti/PbO$_2$-0.2Fe | 0.011 | 0.99 |
| Ti/PbO$_2$-0.05C | 0.005 | 0.96 |
| Ti/PbO$_2$-0.1Fe-0.05C | 0.010 | 0.97 |

acids) [51]. Hu et al. (2015) reported the electrolysis of acid red B azo dye (1 g L$^{-1}$) using Ce-PbO$_2$/C electrode. They found 60.75% decolorization when the applied voltage is 2 V [52]. However, Andrade et al. (2007) found 90% of decolorization of Blue Reactive 19 (25 mg L$^{-1}$) dye using Fe-doped PbO$_2$ (5 cm$^2$) electrode when applying current density of 50 mA cm$^2$ [53].

The curves of Ln ($C_0$/C) versus time for different prepared anodes are shown in Fig. 7b. From the good linear

correlation for all electrodes, the degradation of RY14 followed the pseudo-first-order kinetics according to Eq. 3.

$$C = C_0 e^{-K_{app}\,t}, \tag{3}$$

where $k_{app}$ is the apparent kinetics coefficient.

The pseudo-first-order apparent rate constants ($k_{app}$) of 0.027 min$^{-1}$ and 0.020 min$^{-1}$ were found for Ti/PbO$_2$ and Ti/PbO$_2$-0.1Fe, respectively (Table 4). This indicates that the oxidation power of these two electrodes is higher compared to the others. The better performance for the degradation of RY14 on Ti/PbO$_2$ and Ti/PbO$_2$-0.1Fe can be ascribed to the high oxygen evolution potential, high specific surface area, and good electrical conductivity. These properties allowed the generation of more HO$^{\bullet}$-free radicals which lead to an improvement in the decolorization ability of these anodes [54].

## 4 Conclusion

Fe and/or C-doped Lead dioxide electrodes were prepared onto the pretreated Ti plate by anodic oxidation of solutions containing Fe$^{3+}$ and/or C to Pb$^{2+}$ in the electrodeposition bath. SEM/EDS and XRD tests show that Fe and/or C doping in lead dioxide films can decrease the crystal size of the anodes and increase their specific surface area. The highest OEP is found for the Ti/PbO$_2$-0.1Fe electrode. In the CV test, the presence of the anodic peak for all the prepared electrodes suggests that the oxidation of the RY14 dye was easily achieved on the surface of those anodes studied. Furthermore, the resistance to polarization is found to decrease significantly by adding 0.1 M Fe$^{3+}$ to the prepared carbon-doped anode, indicating the positive effect of iron in promoting the electrochemical reaction process in the presence of carbon. The use of pure and Fe$^{3+}$ (0.1 M)-doped PbO$_2$ electrodes in the decolorization of the RY14 dye proved to be good candidates for the mineralization of the RY14 dye, since more than 90% mineralization was achieved after 2 h of electrolysis.

## Declarations

## References

1. Berradi M, Hsissou R, Khudhair M et al (2019) Textile finishing dyes and their impact on aquatic environs. Heliyon 5:e02711. https://doi.org/10.1016/j.heliyon.2019.e02711

2. Lipskikh OI, Korotkova EI, Khristunova YP et al (2018) Sensors for voltammetric determination of food azo dyes: a critical review. Electrochim Acta 260:974–985. https://doi.org/10.1016/j.electacta.2017.12.027

3. Aguilar ZG, Brillas E, Salazar M et al (2017) Evidence of Fenton-like reaction with active chlorine during the electrocatalytic oxidation of acid yellow 36 azo dye with Ir-Sn-Sb oxide anode in the presence of iron ion. Appl Catal B Environ 206:44–52. https://doi.org/10.1016/j.apcatb.2017.01.006

4. Natarajan R, Manivasagan R (2018) Treatment of tannery effluent by passive uptake: parametric studies and kinetic modeling. Environ Sci Pollut Res 25:5071–5075. https://doi.org/10.1007/s11356-017-9456-9

5. Elshaarawy RFM, Sayed TM, Khalifa HM, El-Sawi EA (2017) A mild and convenient protocol for the conversion of toxic acid red 37 into pharmacological (antibiotic and anticancer) nominees: organopalladium architectures. C R Chim 20:934–941. https://doi.org/10.1016/j.crci.2017.07.003

6. Benkhaya S, Achiou B, Ouammou M et al (2019) Preparation of low-cost composite membrane made of polysulfone/polyetherimide ultrafiltration layer and ceramic pozzolan support for dyes removal. Mater Today Commun 19:212–219. https://doi.org/10.1016/j.mtcomm.2019.02.002

7. Pacheco-Álvarez MOA, Picos A, Pérez-Segura T, Peralta-Hernández JM (2019) Proposal for highly efficient electrochemical discoloration and degradation of azo dyes with parallel arrangement electrodes. J Electroanal Chem 838:195–203. https://doi.org/10.1016/j.jelechem.2019.03.004

8. Bouras HD, Isik Z, Bezirhan Arikan E et al (2019) Photocatalytic oxidation of azo dye solutions by impregnation of ZnO on fungi. Biochem Eng J 146:150–159. https://doi.org/10.1016/j.bej.2019.03.014

9. Shi Q, Chen M, Diao G (2013) Electrocatalytical reduction of m-nitrophenol on reduced graphene oxide modified glassy carbon electrode. Electrochim Acta 114:693–699. https://doi.org/10.1016/j.electacta.2013.10.108

10. Duan X, Zhao Y, Liu W, Chang L (2019) Investigation on electrocatalytic oxidation properties of carbon nanotube-Ce-modified PbO$_2$ electrode and its application for degradation of m-nitrophenol. Arab J Chem 12:709–717. https://doi.org/10.1016/j.arabjc.2014.11.025

11. El Aggadi S, El Abbassi Z, El Hourch A (2021) Color removal from dye-containing aqueous solutions by electrooxidation. Desalin Water Treat 215:232–236. https://doi.org/10.5004/dwt.2021.26766

12. Li D, Tang J, Zhou X et al (2016) Electrochemical degradation of pyridine by Ti/SnO2-Sb tubular porous electrode. Chemosphere 149:49–56. https://doi.org/10.1016/j.chemosphere.2016.01.078

13. El Aggadi S, Kaichouh G, El Abbassi Z, et al (2021) Electrode material in electrochemical decolorization of dyestuffs wastewater: a review. In: E3S Web of Conferences

14. Briega-Martos V, Solla-Gullón J, Koper MTM et al (2019) Electrocatalytic enhancement of formic acid oxidation reaction by acetonitrile on well-defined platinum surfaces. Electrochim Acta 295:835–845. https://doi.org/10.1016/j.electacta.2018.11.016

15. Yin D, Liu Y, Song P et al (2019) In situ growth of copper/reduced graphene oxide on graphite surfaces for the electrocatalytic reduction of nitrate. Electrochim Acta 324:134846. https://doi.org/10.1016/j.electacta.2019.134846

16. Telli E, Döner A, Kardaş G (2013) Electrocatalytic oxidation of methanol on Ru deposited NiZn catalyst at graphite in alkaline medium. Electrochim Acta 107:216–224. https://doi.org/10.1016/j.electacta.2013.05.113

17. Sun Q, Park SJ, Kim S (2015) Preparation and electrocatalytic oxidation performance of Pt/MnO$_2$-graphene oxide nanocomposites. J Ind Eng Chem 26:265–269. https://doi.org/10.1016/j.jiec.2014.12.002

18. Chen Z, Xie G, Pan Z et al (2021) A novel Pb/PbO$_2$ electrodes prepared by the method of thermal oxidation-electrochemical oxidation: characteristic and electrocatalytic oxidation performance. J Alloys Compd 851:156834. https://doi.org/10.1016/j.jallcom.2020.156834

19. Souri Z, Ansari A, Nematollahi D, Mazloum-Ardakani M (2020) Electrocatalytic degradation of dibenzoazepine drugs by fluorine doped β-PbO$_2$ electrode: new insight into the electrochemical oxidation and mineralization mechanisms. J Electroanal Chem 862:114037. https://doi.org/10.1016/j.jelechem.2020.114037

20. Park HS, Yang J, Cho MK et al (2019) RuO$_2$ nanocluster as a 4-in-1 electrocatalyst for hydrogen and oxygen electrochemistry. Nano Energy 55:49–58. https://doi.org/10.1016/j.nanoen.2018.10.017

21. Ha Y, Jung H, Lee C et al (2015) Alteration of the morphology and electrocatalytic activity of IrO$_2$ nanowires upon reduction by hydrogen gas. Sens Actuators B Chem 216:159–164. https://doi.org/10.1016/j.snb.2015.04.037

22. Wang W, Duan X, Sui X et al (2020) Surface characterization and electrochemical properties of PbO$_2$/SnO$_2$ composite anodes for electrocatalytic oxidation of m-nitrophenol. Electrochim Acta 335:135649. https://doi.org/10.1016/j.electacta.2020.135649

23. Shestakova M, Graves J, Sitarz M, Sillanpää M (2016) Optimization of Ti/Ta$_2$O$_5$-SnO$_2$ electrodes and reaction parameters for electrocatalytic oxidation of methylene blue. J Appl Electrochem 46:349–358. https://doi.org/10.1007/s10800-016-0925-5

24. Bai H, He P, Pan J et al (2017) Boron-doped diamond electrode: Preparation, characterization and application for electrocatalytic degradation of m-dinitrobenzene. J Colloid Interface Sci 497:422–428. https://doi.org/10.1016/j.jcis.2017.03.017

25. Zhao B, Yu H, Lu Y et al (2019) Polyethylene glycol assisted synthesis of a praseodymium-doped PbO$_2$ electrode and its enhanced electrocatalytic oxidation performance. J Taiwan Inst Chem Eng 100:144–150. https://doi.org/10.1016/j.jtice.2019.04.015

26. Shmychkova O, Luk'yanenko T, Yakubenko A et al (2015) Electrooxidation of some phenolic compounds at Bi-doped PbO$_2$. Appl Catal B Environ 162:346–351. https://doi.org/10.1016/j.apcatb.2014.07.011

27. Velichenko AB, Amadelli R, Zucchini GL et al (2000) Electrosynthesis and physicochemical properties of Fe-doped lead dioxide electrocatalysts. Electrochim Acta 45:4341–4350. https://doi.org/10.1016/S0013-4686(00)00538-7

28. Hao X, Dan S, Qian Z et al (2014) Preparation and characterization of PbO$_2$ electrodes from electro-deposition solutions with different copper concentration. RSC Adv 4:25011–25017. https://doi.org/10.1039/c4ra03235g

29. Yao Y, Zhao M, Zhao C, Zhang H (2014) Preparation and properties of PbO$_2$-ZrO$_2$ nanocomposite electrodes by pulse electrodeposition. Electrochim Acta 117:453–459. https://doi.org/10.1016/j.electacta.2013.11.150

30. Wang Z, Xu M, Wang F et al (2017) Preparation and characterization of a novel Ce doped PbO$_2$ electrode based on NiO modified Ti/TiO$_2$NTs substrate for the electrocatalytic degradation of phenol wastewater. Electrochim Acta 247:535–547. https://doi.org/10.1016/j.electacta.2017.07.057

31. Andrade LS, Rocha-Filho RC, Bocchi N et al (2008) Degradation of phenol using Co- and Co, F-doped PbO$_2$ anodes in electrochemical filter-press cells. J Hazard Mater 153:252–260. https://doi.org/10.1016/j.jhazmat.2007.08.046

32. Velichenko AB, Devilliers D (2007) Electrodeposition of fluorine-doped lead dioxide. J Fluor Chem 128:269–276. https://doi.org/10.1016/j.jfluchem.2006.11.010

33. Hao X, Quansheng Y, Dan S et al (2015) Fabrication and characterization of PbO$_2$ electrode modified with [Fe(CN)$_6$]$^{3-}$ and its application on electrochemical degradation of alkali lignin. J Hazard Mater 286:509–516. https://doi.org/10.1016/j.jhazmat.2014.12.065

34. Duan X, Ma F, Yuan Z et al (2012) Comparative studies on the electro-catalytic oxidation performance of surfactant-carbon nanotube-modified PbO$_2$ electrodes. J Electroanal Chem 677–680:90–100. https://doi.org/10.1016/j.jelechem.2012.05.012

35. Li X, Xu H, Yan W (2017) Effects of 12 sodium dodecyl sulfate (SDS) on electro-catalytic performance and stability of PbO$_2$ electrode. J Alloys Compd 718:386–395. https://doi.org/10.1016/j.jallcom.2017.05.147

36. Velichenko A, Luk'yanenko T, Shmychkova O (2020) Lead dioxide-SDS composites: design and properties. J Electroanal Chem. https://doi.org/10.1016/j.jelechem.2020.114412

37. Duan X, Xu F, Wang Y et al (2018) Fabrication of a hydrophobic SDBS-PbO$_2$ anode for electrochemical degradation of nitrobenzene in aqueous solution. Electrochim Acta 282:662–671. https://doi.org/10.1016/j.electacta.2018.06.098

38. Li X, Xu H, Yan W (2016) Fabrication and characterization of PbO$_2$ electrode modified with polyvinylidene fluoride (PVDF). Appl Surf Sci 389:278–286. https://doi.org/10.1016/j.apsusc.2016.07.123

39. Yang W, Yang W, Lin X (2012) Research on PEG modified Bi-doping lead dioxide electrode and mechanism. Appl Surf Sci 258:5716–5722. https://doi.org/10.1016/j.apsusc.2012.02.073

40. Ju P, Fan H, Guo D et al (2012) Electrocatalytic degradation of bisphenol A in water on a Ti-based PbO$_2$-ionic liquids (ILs) electrode. Chem Eng J 179:99–106. https://doi.org/10.1016/j.cej.2011.10.065

41. Zhang L, Xu L, He J, Zhang J (2014) Preparation of Ti/SnO$_2$-Sb electrodes modified by carbon nanotube for anodic oxidation of dye wastewater and combination with nanofiltration. Electrochim Acta 117:192–201. https://doi.org/10.1016/j.electacta.2013.11.117

42. Zhang G, Sun S, Yang D et al (2008) The surface analytical characterization of carbon fibers functionalized by H$_2$SO$_4$/HNO$_3$ treatment. Carbon N Y 46:196–205. https://doi.org/10.1016/j.carbon.2007.11.002

43. Feng M, Wang S, Yu Y et al (2017) Carboxyl functionalized carbon fibers with preserved tensile strength and electrochemical performance used as anodes of structural lithium-ion batteries. Appl Surf Sci 392:27–35. https://doi.org/10.1016/j.apsusc.2016.09.017

44. Baddouh A, Bessegato GG, Rguiti MM et al (2018) Electrochemical decolorization of Rhodamine B dye: influence of anode material, chloride concentration and current density. J Environ Chem Eng 6:2041–2047. https://doi.org/10.1016/j.jece.2018.03.007

45. Souza FL, Aquino JM, Irikura K et al (2014) Electrochemical degradation of the dimethyl phthalate ester on a fluoride-doped Ti/β-PbO$_2$ anode. Chemosphere 109:187–194. https://doi.org/10.1016/j.chemosphere.2014.02.018

46. Hao X, Wuqi G, Jia W et al (2016) Preparation and characterization of titanium-based PbO$_2$ electrodes modified by ethylene glycol. RSC Adv 6:7610–7617. https://doi.org/10.1039/c5ra21195f

47. Shmychkova O, Luk'yanenko T, Velichenko A et al (2013) Bi-doped PbO$_2$ anodes: electrodeposition and physico-chemical properties. Electrochim Acta 111:332–338. https://doi.org/10.1016/j.electacta.2013.08.082

48. Xu A, Dai X, Wei K et al (2017) Preparation and characterization of a TiO$_2$-NT/SnO$_2$-Sb tubular porous electrode with long service lifetime for wastewater treatment process. RSC Adv 7:37806–37814. https://doi.org/10.1039/c7ra05127a

49. Zhang C, Liu J, Chen B (2019) Effect of Ce(NO$_3$)$_4$ on the electrochemical properties of Ti/PbO$_2$-TiO$_2$-Ce(NO$_3$)$_4$ electrode for zinc electrowinning. Appl Phys A Mater Sci Process 125:1–7. https://doi.org/10.1007/s00339-019-2462-7

50. Li X, Xu H, Yan W (2016) Fabrication and characterization of PbO$_2$ electrode modified with polyvinylidene fluoride (PVDF). Appl Surf Sci 389:278–286

51. Zaidi SZJ, Harito C, Walsh FC, Ponce de León C (2018) Decolourisation of reactive black-5 at an RVC substrate decorated with PbO$_2$/TiO$_2$ nanosheets prepared by anodic electrodeposition. J Solid State Electrochem 22:2889–2900. https://doi.org/10.1007/S10008-018-3992-1/FIGURES/11

52. Hu X, Yu Y, Yang L (2015) Electrocatalytic activity of Ce-PbO$_2$/C anode for acid red B reduction in aqueous solution. J Solid State Electrochem 196(19):1599–1609. https://doi.org/10.1007/S10008-015-2781-3

53. Andrade LS, Ruotolo LAM, Rocha-Filho RC et al (2007) On the performance of Fe and Fe, F doped Ti-Pt/PbO$_2$ electrodes in the electrooxidation of the blue reactive 19 dye in simulated textile wastewater. Chemosphere 66:2035–2043. https://doi.org/10.1016/J.CHEMOSPHERE.2006.10.028

54. Li X, Xu H, Yan W (2016) Preparation and characterization of PbO$_2$ electrodes modified with polyvinyl alcohol (PVA). RSC Adv 6:82024–82032. https://doi.org/10.1039/c6ra17230j